FePd nanowires modified with cyclodextrin. Characterization and catalytic properties evaluated by a model reduction reaction.

Elisa Herrera,[a] M. Soledad Aprea,[b] Julieta S. Riva,[c] O. Fernando Silva,[a] Paula G. Bercoff,[b] and Alejandro Granados[a*]

a Universidad Nacional de Córdoba. Facultad de Ciencias Químicas Departamento de Química Orgánica. Instituto de Investigaciones en Fisicoquímica de Córdoba, INFIQC
Haya de la Torre esq. Medina Allende, Ciudad Universitaria, CP:X5000HUA, Córdoba, Argentina.
b Universidad Nacional de Córdoba. Facultad de Matemática, Astronomía, Física y Computación. CONICET, IFEG. Av. Medina Allende s/n, Ciudad Universitaria, CP:X5000HUA, Córdoba, Argentina
c Instituto de Investigaciones en Fisicoquímica de Córdoba, INFIQC-CONICET. Haya de la Torre esq. Medina Allende, Ciudad Universitaria, CP:X5000HUA, Córdoba, Argentina *ale@fcq.unc.edu.ar

Abstract

FePd and Pd nanowires (NWs), were synthesized by electrodeposition into a nanoporous alumina membrane and superficially functionalized with a modified β-cyclodextrin (βCDMOD14). A complete description is provided, at the molecular level, of the modified surface supported by FT-IR and XPS spectroscopy data. FePd NWs@βCDMOD14 showed excellent catalytic activity in the reduction reaction of 4-nitrophenol with $NaBH_4$, being 10 times higher than NWs without βCDMOD14 and even better than Pd NWs@βCDMOD14.

Keywords: Surface modification • magnetic properties • XPS • EDS • 4-nitrophenol

1. Introduction

Among the metals widely used as catalysts, Pd emerges as an excellent alternative to other more expensive and scarce sources such as Pt.[1] In this regard, Pd has been intensively studied over the last three decades.[2,3]This catalyst was successfully employed in chemical reactions of great interest in the green chemistry area, for example in the reduction of pollutants such as 4-nitrophenol (4-NP) or in the sustainable energy and fuel area, as promising candidates for oxygen reduction reaction (ORR) in the fuel cells.[4] Also, it is known that nanostructures in general are of great interest in the catalysis area due to their high surface/volume ratio.[2,5] Bimetallic nanoparticles in which a magnetic metal is added, have the advantage of being recovered from the reaction medium with the aid of external magnets. Also, in some cases, synergistic effects between the metals in the catalytic behavior are postulated.[6]

Since the catalytic behavior of the nanocatalysts is determined by their characteristics, composition, morphology, dimensions and crystallinity,[7,8] a complete characterization of the used nanostructures is crucial.[1,6] On the other hand, electrodeposition into the ordered pores of anodic aluminum oxide (AAO) membranes is not only a low-cost synthesis technique, but it also allows to control the attributes of the catalysts by altering the electrochemical deposition parameters.[9,10] However, it is acknowledged that one of the disadvantages of using metallic nanostructures as catalysts is the tendency to coalesce and form large particles when they are dispersed in aqueous solution. This agglomeration decreases the number of surface metal atoms per unit mass of metal, and thereby reduces the catalyst activity.[11] In order to avoid that phenomenon, a stabilizer has to be added on the

surface of the nanostructure. Cyclodextrins (CDs) are compounds constituted by α-D-glucose units bound by glycosidic α-1,4 bonds, and depending on the number of units that form them they are called: αCD, for six units, βCD for seven and γCD for eight glucose units. They have a hydrophobic internal cavity and a hydrophilic external surface, which represent an accessible, clean and non-toxic approach to confer colloidal stability preventing the aggregation of nanostructures since they are easily adsorbed on the surface.[12,13] Although there are a large number of examples in the literature employing CDs and their derivatives to stabilize nanoparticles,[13,14] to the best of our knowledge only one previous work has proposed the use of CDs with nanowires (NWs).[2]

In this work, we present results referred to the reduction reaction of 4-NP with $NaBH_4$ in aqueous medium[15,16] mediated by FePd and Pd NWs, synthesized by electrodeposition, and modified with a βCD derivative (βCDMOD14, see Scheme 1).[17] The discussion is centered on the structural and magnetic properties, surface modification and catalytic activity of the NWs. The main contribution of our research is to show that nanostructures with high catalytic activity can achieved combining a simple electrodeposition method with an even easier post-synthetic modification strategy for improving surface properties. This approach has the potential to open new routes and possible applications of new materials that can replace expensive metals in catalytic reactions.

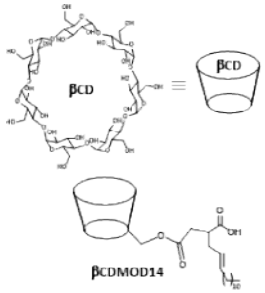

Scheme 1. βCD and βCDMOD14schematic representation.

2. Material and methods

The NWs used in this study were obtained by template-assisted electrodeposition using commercial AAO membranes of 200 nm pore diameter. For synthesizing Pd NWs a 0.04 M $PdCl_2$ solution was used, while a 0.05 M $FeCl_3$ + 0.02 M $PdCl_2$ electrolyte was employed for the synthesis of FePd NWs. The supporting electrolyte was ammonium citrate, and ammonium hydroxide was added to the solution to keep the pH = 9.00. The potential for the electrodeposition was -1.5V *vs*. Ag/AgCl, and the deposition time was 30 minutes.

EDS results were obtained by taking the average of several spectra measured in different areas of each sample.

To release the NWs from the alumina template, after XRD and magnetic characterizations, each template was kept in a 0.1 M NaOH solution for 6 h. Then, the NWs were rinsed with water twice, retaining them at the bottom of the vial with a permanent magnet while removing the water. After the last rinse, a βCDMOD14, 5×10^{-4} M solution at pH 9.0 was added; the NWs were kept for 24 h in this medium. After this lapse, the excess of βCDMOD14 solution was removed, obtaining the modified NWs, denoted NWs@βCDMOD14. Finally, the NWs@βCDMOD14 were easily dispersed in 2 mL of deionized water. The presence of βCDMOD14 on the surface of the NWs was confirmed by Infrared Spectroscopy, Attenuated Total Reflection (IR-ATR) and X-ray Photoelectron Spectrometry (XPS).

A schematic representation of the entire process of synthesis, surface modification, and

characterization is shown in **Fig. S1(a)**.

3. Results and Discussion

The chemical compositions of the resulting NWs were determined by Energy Dispersive Spectrometry (EDS) after dissolving the alumina template. The alloy composition of the bimetallic NWs is $Fe_{55}Pd_{45}$ and Pd NWs are pure, as can be confirmed from the representative spectra shown in **Fig. S2**.

Fig. 1 a and **b** show Scanning Electron Microscope (SEM) images of FePd and Pd NWs, respectively. Several SEM images let estimate the NWs diameter of approximately 200 nm ─the same as the pore diameter of the alumina template─ and NWs lengths of 13 µm for FePd NWs and 10 µm for Pd NWs. **Fig. 1 c** displays a bright field transmission electron microscope (TEM) image of a FePd NW, where the mean diameter of 200 nm is confirmed and a granular microstructure is evident.

The crystalline structure of the as-electrodeposited NWs was studied by X-ray diffraction (XRD) and the corresponding diffractograms are shown in **Fig. 2**. In both samples only the reflections of the *fcc* crystalline structure are detected, indicating no secondary phases are present within the detection limit

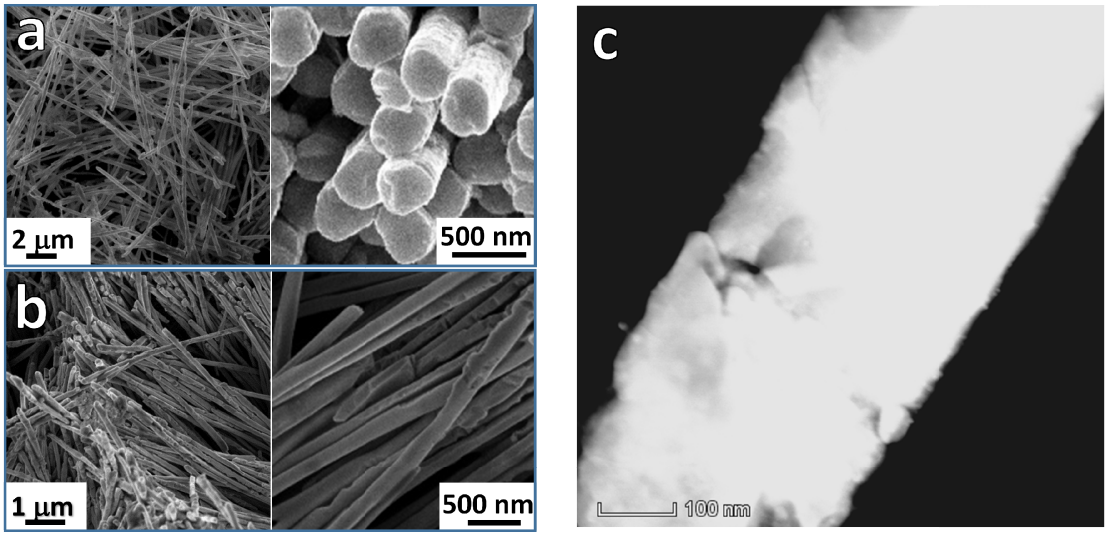

Figure 1. SEM images of (a) FePd and (b) Pd NWs after being released from the AAO templates. (c) TEM image of a FePd NW, where a granular microstructure can be seen.

of this technique. The amorphous structure of the alumina template in which the NWs were kept for the measurement originates a large bump in the patterns, which is distributed in a wide range of angles. The pure Pd NWs have a cubic *fcc* structure with a cell parameter a_{Pd}=3.893Å and grow preferentially along the (022) crystalline direction, which corresponds to the reflection peak at 2θ=68.44°. For FePd NWs, the peaks observed around 41°, 47° and 68° are associated to the family of planes (111), (200), (220) of a γ-FePd disordered *fcc* structure. The cell parameter a_{FePd}=3.838 Å indicates that in these NWs, Fe and Pd are indeed alloyed.[18] The average crystallite size in each sample was calculated using the Scherrer formula, resulting in (6±2) nm and (15±3) nm for FePd and Pd NWs, respectively. This indicates that the NWs have a granular microstructure, in agreement with TEM rsults.

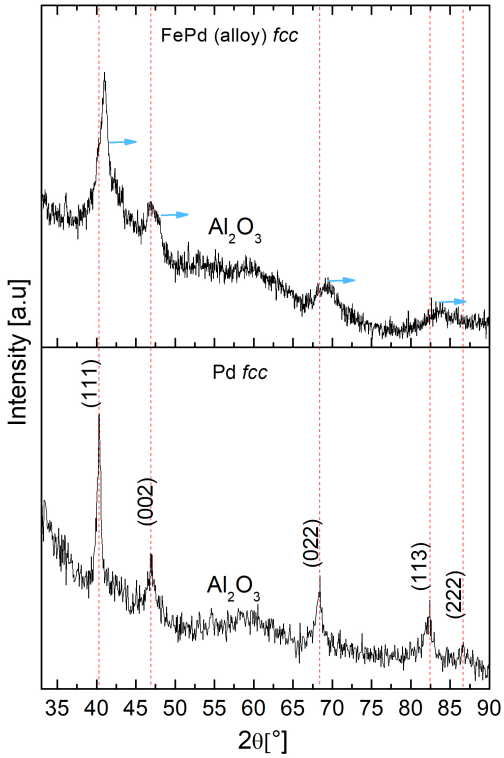

Figure 2. X-ray diffractograms of as-deposited NWs arrays within the AAO templates. The vertical dashed lines mark the positions of the theoretical reflections that correspond to the *fcc* phase of pure Pd. The horizontal arrows in the alloy's pattern indicate the peaks displacement with respect to pure Pd as a result of the change in cell parameter. No secondary phases are detected.

Fig. S3 shows the room temperature magnetic hysteresis loops corresponding to FePd and Pd NWs arrays. Pd NWs show paramagnetic behavior (**Fig. S3b**). In the case of FePd NWs arrays, the normalized magnetization M/Ms (being Ms the saturation magnetization) is measured with the applied magnetic field parallel (PA) and perpendicular (PE) to the NWs long axis. As it can be seen in **Fig. S3a**, the NWs are soft ferromagnetic (coercivity $\approx$10 mT for both PA and PE configurations) with a fast response to an external magnetic field, allowing an easy magnetic manipulation. It was found that the magnetic easy axis is parallel to the long NWs axis, which is usually the preferred direction in one-dimensional nanostructures, when shape anisotropy is dominant.[19]

The surface of the NWs was modified with βCDMOD14, which was confirmed by Infrared Spectroscopy, Attenuated Total Reflection (IR-ATR) and X-ray Photoelectron Spectrometry (XPS). In **Fig. 3**, the FT-IR spectrum of pure βCDMOD14 shows the presence of two characteristic bands at 3425 cm^{-1} and 2950 cm^{-1}, which are attributed to the stretching vibration of the O-H and the C-H bonds, respectively. These bands are also observed in the FT-IR spectrum of FePdNWs@βCDMOD14, with small differences both in shifting and in their relative intensities. The most significant changes are observed in the range of 1000 to 1700 cm^{-1}. The band associated with the stretching mode of the C=O groups of βCDMOD14, shifts from 1734 cm^{-1} to 1620 cm^{-1} in the coated NWs, which is attributed to the interaction of the carboxylic group with the surface of NWs. The most remarkable

change is the important decrease in the relative intensities of the bands observed at 1150, 1083 and 1030 cm^{-1} compared with the corresponding peaks of the βCDMOD14 spectrum. These bands have been assigned to certain vibration modes of the O-C-O bonds of the βCD skeleton as well as both primary and secondary C-OH.[20] The suppression of these vibration modes reveals the role of the CD ring in the interactions between βCDMOD14 and NWs surfaces, in agreement with what was proposed through all-atom molecular dynamics simulations for the adsorption of βCD on the surface of gold nanoparticles.[21]

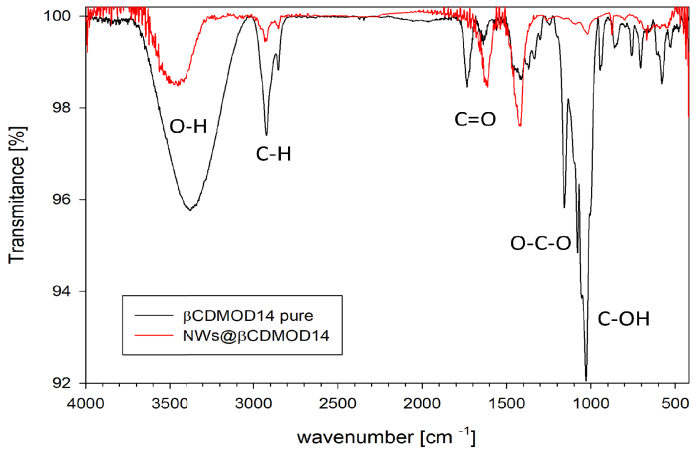

Figure 3. FT-IR spectrum of FePd NW@βCDMOD14 compared with that obtained for pure βCDMOD14. The presence of two characteristic bands at 3425 cm^{-1} and 2950 cm^{-1} are observed, which are attributed to the stretching vibration of the OH and the C-H bond, respectively. These bands also appear in the spectrum of the NWs with small differences both in shifting and in their relative intensities. The broad band at ~1620 cm^{-1} was associated to different vibrational modes of the carboxyl group of βCDMOD14 with the metallic surface.[22,23]

Fig. S4 shows the XPS survey spectrum of FePdNWs@βCDMOD14 where the C, O, Fe and Pd fingerprints can be observed. **Fig. S5** displays high resolution spectra of C1s and O1s comparing pure βCDMOD14, FePd NWs and FePdNWs@βCDMOD14. The presence of C and O peaks in the samples spectra could be originated either by βCDMOD14 or by adventitious contamination of carbonaceous substances and the formation of iron oxides on the surface. Therefore, for a deeper knowledge of the NWs surface, it is necessary to analyze the high resolution spectra for each energy zone. The deconvolution of the peaks, shown in **Fig. 4**, allows obtaining information to account for the different atomic environments for each element. The atomic percentage of each type of C and O atom, obtained experimentally from the relative areas of experimental XPS deconvoluted peaks, are in agreement with the values calculated from the βCDMOD14 molecular structure (see **Scheme 1**). In the C 1s zone (left panel of **Fig. 4**) the peaks at 284.8 eV, 286.0 eV, 287.9 eV and 289.6 eV correspond to C-C, C-O, O-C-O and O-C=O bonds, respectively,[24,25] and appear in pure βCDMOD14 (**Fig. 4a**) and in FePdNWs@βCDMOD14 (**Fig. 4b**), as was expected. These contributions were not observed in the spectrum of NWs without βCDMOD14, where only the signal of adventitious C is present at 284.8 eV (**Fig. 4c**). In the O 1s zone (right panel of **Fig. 4**), the peaks at

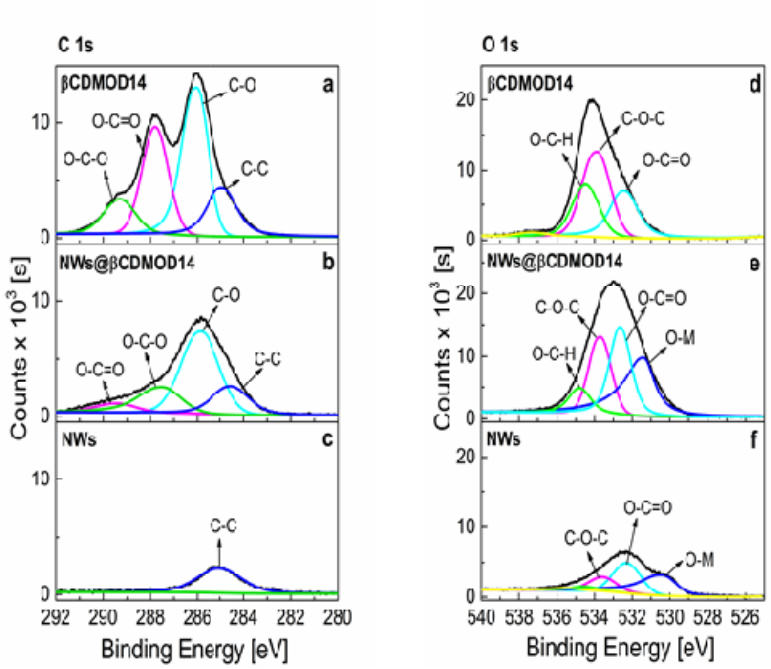

Figure 4. Deconvolution of XPS spectra corresponding to band C 1s for (a) pure βCDMOD14, (b) FePdNWs@βCDMOD14 and (c) FePd NWs. Deconvolution of band O 1s for (d) pure βCDMOD14, (e) FePdNWs@βCDMOD14 and (f) FePd NWs.

529.5 eV, 531.0 eV, 532.0 eV and 532.9 eV were assigned to C=O, O-C=O, HO-C and C-O bonds respectively.[26–29] The peaks corresponding to O-C=O and C-O-C bonds in the spectrum of βCDMOD14 (**Fig. 4d**) remain constant or slightly decrease in the spectrum of FePdNWs@βCDMOD14 (**Fig. 4e**). Besides, the contributions of the C-O-H and C-O-C bonds diminished and the signal attributed to the O-metal interaction increases in FePd NWs@βCDMOD14. In FePd NWs without βCDMOD14 (**Fig. 4f**), the O 1s contribution is weaker than the obtained for pure βCDMOD14 (**Fig. 4d**) or FePd NWs@βCDMOD14 (**Fig. 4e**), which indicates that there was less oxygen in the former mentioned surface. The signal at 529 eV observed for FePd NWs (**Fig. 4f**) is attributed to iron oxide,[30] and it is also observed for FePd NWs@βCDMOD14 (**Fig. 4e**). These results confirm the presence of βCDMOD14 on the surface of the NWs and suggest that C-O-C and OH groups are involved in that union as was suggested by the changes observed in the IR spectra discussed above. This also agrees with that proposed by others authors regarding the interaction mode of CDs with different metal surfaces.[21] **Fig. 5a** shows the high resolution XPS spectra for Pd 3d signal corresponding to NWs still in the template, after removing the template and with modified surface by βCDMOD14. In all cases, the signals are the corresponding to metallic Pd, 335.1eV and 340.5eV. However, the broadening of the peaks towards higher energies in the case of NWs@βCDMOD14 would be indicating interaction of the Pd with oxygen atoms of the βCDMOD14 [4,31].

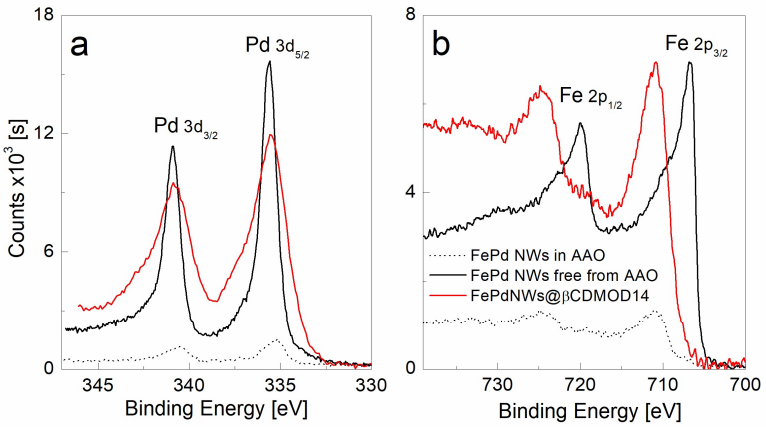

Figure 5. High resolution XPS spectra of as-obtained NWs (dotted line), after removing from the AAO template (black solid line) and NWs@βCDMOD14 (red solid line) for Pd 3d(a) and Fe 3p(b) regions respectively.

Fig. 5b also compares the high resolution XPS spectra corresponding to the Fe 2p signals. The shift of the peaks corresponding to NWs@βCDMOD14 towards higher energies, compared to the bare NWs, indicates that the Fe in the former is in a much more oxygenated environment. This is compatible with the interaction with βCDMOD14 oxygen atoms and the presence of iron oxide.

The reduction of 4-NP to 4-aminophenol (4-AP) has been frequently used as a model reaction in order to evaluate the catalytic activity of nanostructures, due to the simple way in which the progress of the reaction can be accurately followed by UV-vis spectroscopy.[32–34] Therefore, the catalytic activity of the NWs synthesized in this work was determined by the aforementioned model reaction.

The UV-vis spectra of the mixture of 10^{-4} M 4-NP and 0.1 M $NaBH_4$ with FePd NWs@βCDMOD14 for different times are shown in **Fig. 6**, where a strong absorption peak at around 400 nm ─ attributed to 4-nitrophenolate anion─ can be observed. The main peak at 400 nm decreases as the reaction time proceeds, and a band centered at 300 nm appears, corresponding to the product 4-AP. The occurrence of an isosbestic point at 314 nm indicates that there is no accumulation of any reaction intermediate (see **Fig. 6**). By measuring absorbance values at 400 nm during the reaction (Abs_t) and plotting $\ln(Abs_t/Abs_{t=0})$ as a function of time t, the rate constant k_{obs}, can be obtained from the slope of this linear relation, assuming that the reaction is carried out under pseudo first order conditions.

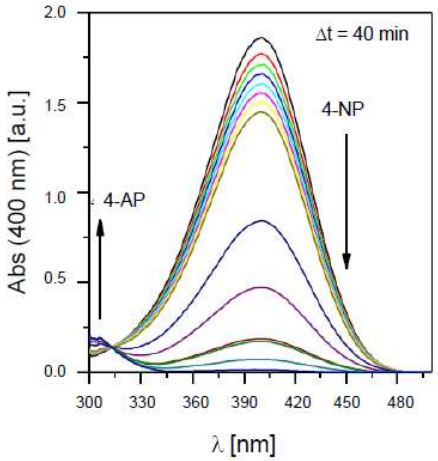

Figure 6. UV-vis spectra at different times of the reduction reaction of 4-NP 10^{-4} M in aqueous solution containing $NaBH_4$ 0.1 M and FePd NWs@βCDMOD14.

The parameter S used in heterogeneous catalysis is defined as the catalyst area per volume of reaction medium and is calculated from the geometrical and physical parameters of the catalyst (length and diameter of the NWs, density, molecular weight, and mass of catalyst used) and the final volume of the reaction medium. In order to compare different catalysts it is useful to calculate the ratio k_{obs}/S[35], since this quantity is independent from geometrical factors and the mass of catalyst used. The previously mentioned reduction reaction was carried out with FePd NWs, Pd NWs@βCDMOD14 and FePd NWs@βCDMOD14 using the same concentration of reactants. The k_{obs}/S values obtained for these catalysts are listed in Table 1. For comparison, we also include in this table the experimental catalytic data reported in the literature referring to other Pd-based nanocatalysts.[5,36,37]

Table 1. k_{obs}/S values for the different assessed catalysts.

Catalyst	k_{obs}/S [L s^{-1} m^{-2}]	Ref.
FePd NWs	0.05±0.01	This work
Pd NWs@βCDMOD14	0.20±0.02	This work
FePd NWs@βCDMOD14	0.66±0.02	This work
Pd NPs@βCDMOD14	0.0015±0.0007	Ref 36
Fe_xO_y/Pd NWs@ mesoporous SiO_2	0.162±0.002	Ref 37
Pd-Ni/rGO NPs	0.008±0.003	Ref 5

Taking into account the results listed in Table 1, it is clear that the NWs surface modification significantly improves their catalytic activity. This modification increased the catalytic activity of FePd NWs@βCDMOD14 by a factor of over 10 as compared to the FePd NWs. The explanation we propose for this is that βCDMOD14 avoids the agglomeration of NWs in aqueous medium, leaving most of the catalyst surface available for reactants and therefore providing significant benefit on the final catalytic properties (the photograph of the FePd NWs and FePd NWs@βCDMOD14 suspensions displayed in **Fig. S1 (b)** shows the improved dispersion stability when the NWs are functionalized). However, the fact that 4-NP may have a greater affinity for the metal surface due to the coating with βCDMOD14 cannot be ruled out as a complementary process that leads to the increase in the catalytic capacity of the NWs with modified surface. Although a detailed discussion of the reaction mechanism is beyond the scope of this paper, it was proposed in the literature that the reduction reaction kinetics of 4-NP is influenced by the amount of 4-nitro-phenolate ions and BH_4^- adsorbed onto the surface of the catalyst where they react.[38] It would seem that βCDMOD14 provides an additional site to anchor 4-NP at the surface forming a complex 4-NP with the cavity of cyclodextrins.[36,39] As suggested by Fountoulaki et al.,[40] the rate limiting step is the reduction of one of the formed intermediates, namely 4-hydroxylamine phenol; hence it seems reasonable that this enhancement in catalytic behavior is attributed to the stabilization of the transition state due to the hydrogen bonds between the guest and the βCD host. Analogously, this stabilizing factor was observed in our previous work using palladium nanoparticles coated with βCDMOD14.[36]

Even when Pd NWs@βCDMOD14 and FePd NWs@βCDMOD14 have similar colloidal stability, it is

clear that the presence of iron in the structure is a favorable factor for the catalytic activity, as it has already been proposed by other authors,[6] since it improves the k_{obs}/S ratio over 3 times. Finally, the performance of FePd NWs@βCDMOD14 was also compared with that of other nanocatalysts reported for the 4-NP reduction reaction, assuming that in every case at least 0.1 M of $NaBH_4$ was used as the reducing agent.[6,34,36,37] FePd NWs@βCDMOD14 shows an improved k_{obs}/S ratio than Pd NPs@βCDMOD14 (NPs=nanoparticles)[36], Pd-Ni/rGO[5] and FexOy/Pd NWs@mesoporous SiO_2[37] as displayed in Table 1. FePd NWs@βCDMOD14 synthesized and characterized in this work have the advantage of being magnetically retrievable and also less expensive than their pure Pd NWs counterpart, since over 50% of the metal content corresponds to iron, which considerably decreases the cost of the catalyst.

4. Conclusion

FePd and Pd NWs were synthesized and characterized before and after modifying their surfaces with βCDMOD14. The binding of βCDMOD14 to the NWs surface was confirmed by FT-IR and XPS, showing an important participation of the carboxylate groups and of the cyclodextrin skeleton as binding sites to the metal surface. FePd NWs@βCDMOD14 exhibited an increase of the catalytic activity by a factor of over 10 when compared to the FePd NWs. This effect is attributed to a better colloidal stability in an aqueous medium leaving a greater surface area available for catalysis. FePd NWs@βCDMOD14 showed a better performance than Pd NWs@βCDMOD14, and a similar or even better one than other catalysts reported in the literature for the assayed model reaction.

5. Acknowledgments

CONICET by projects N° PIP2015 112 201501 00515 CO and PUE-2017 CONICET N° 22920170100092, SECyT-UNC by Project Nº 33620180100374CB.

SUPPLEMENTARY INFORMATION

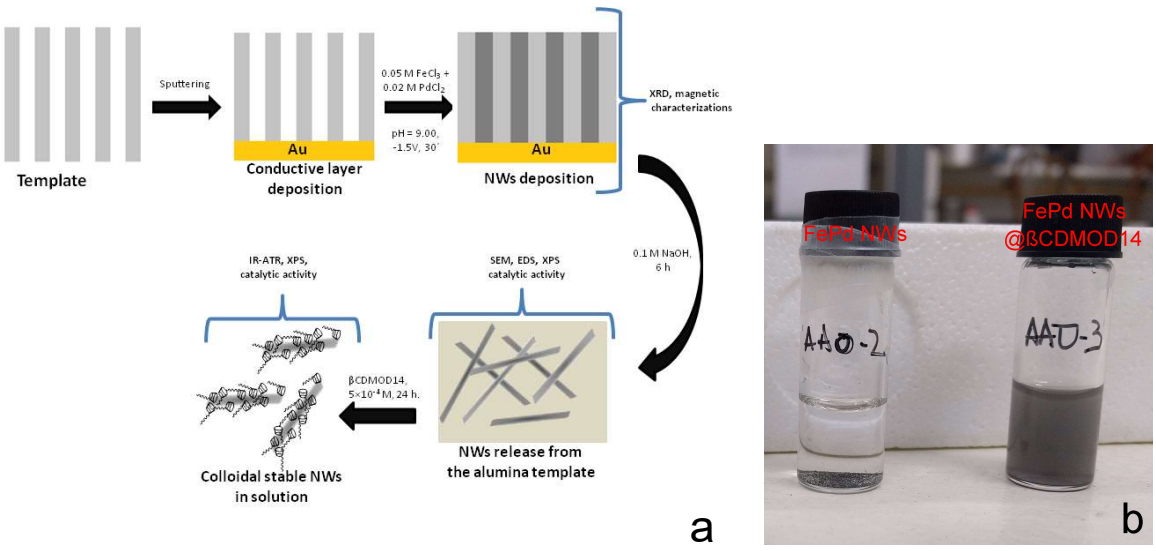

Figure S1. (a) Schematic representation of the entire process: synthesis, characterization and surface modification. **(b)** FePd NWs and FePd NWs@βCDMOD14 suspensions, showing improved dispersion stability when the NWs are functionalized.

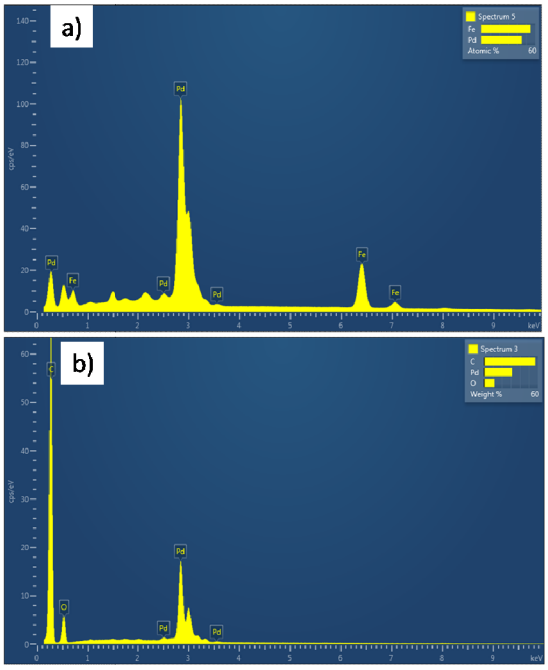

Figure S2. EDS spectra of (a) FePd NWs and (b) Pd NWs after being released from the AAO template.

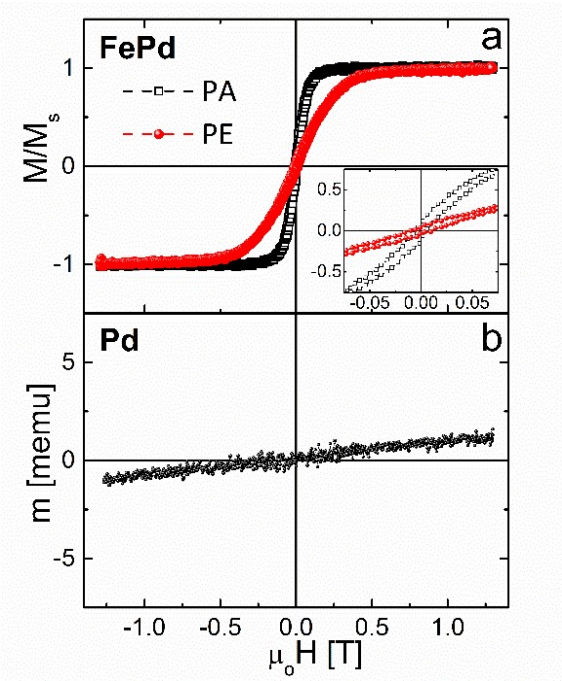

Figure S3. (a) Hysteresis loops of FePdNWs measured parallel (PA) and perpendicular (PE) to the applied magnetic field. Inset: Zoom of the low-field region. (b) Pd paramagnetic behavior.

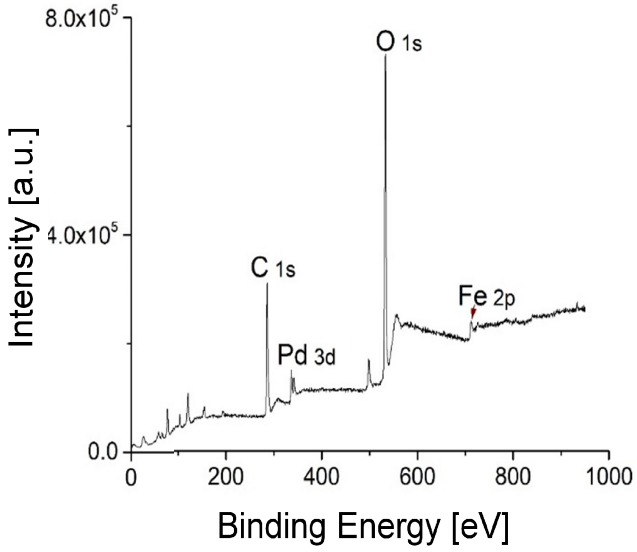

Figure S4. Survey spectrum of FePd NWs@βCDMOD14.

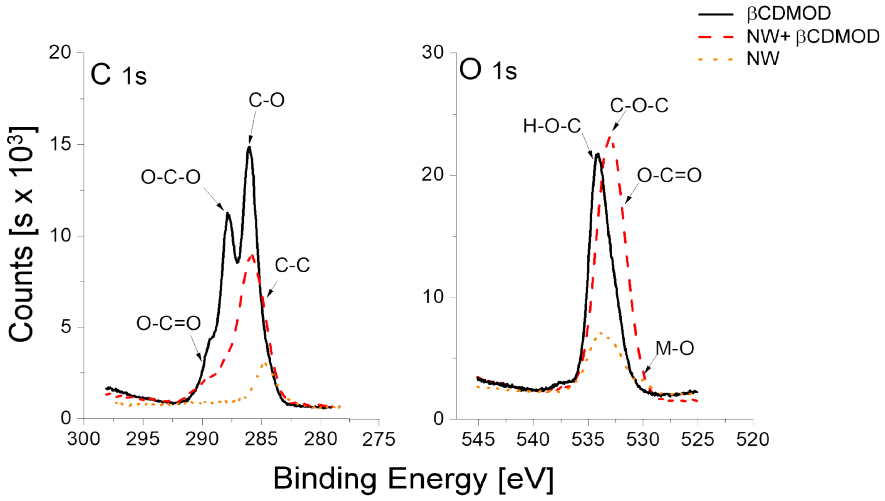

Figure S5: XPS spectra of C (left) and O (rigth) for β-CDMOD14 (black solid line), FePd NWs (red dotted line) and FePd NWs@βCDMOD14 (red dashed line). The signal intensity of C and O in the FePd NWs@βCDMOD14 spectra accounts for the presence of molecules which contain these atoms on the surface of the NWs. This signal largely exceeds the signal intensity expected for adventitious C or O, wich is observed in the spectrum of FePd NWs. Finally, when the C spectra of the three samples are compared, the correspondence between the signals of NWs + CD and CD is clear.

Experimental details

Pristine Pd NWs were not used in the comparison since these nanostructures showed very low colloidal stability.

6. References

[1] V.R. Stamenkovic, B. Fowler, B.S. Mun, G. Wang, P.N. Ross, C.A. Lucas, N.M. Markovic, Improved Oxygen Reduction Activity on Pt3Ni(111) via Increased Surface Site Availability, Science (80-.). 315 (2007) 493–497. https://doi.org/10.1126/science.1135941.

[2] A. Tomer, B.T. Kusema, J.F. Paul, C. Przybylski, E. Monflier, M. Pera-Titus, A. Ponchel, Cyclodextrin-assisted low-metal Ni-Pd/Al 2 O 3 bimetallic catalysts for the direct amination of aliphatic alcohols, J. Catal. 368 (2018) 172–189. https://doi.org/10.1016/j.jcat.2018.10.002.

[3] Q. Ma, N. Wang, G. Liu, L. Wang, Enhanced performance of Pd nanoparticles on SBA-15 grafted with alkyltrialkoxysilane in 2-ethyl-anthraquinone hydrogenation, Microporous Mesoporous Mater. 279 (2019) 245–251. https://doi.org/10.1016/j.micromeso.2018.12.037.

[4] H. Wang, C. Wang, L. Liu, T. Qu, D. Wang, Z. Kang, Synthesis of Co-Fe-Pd nanoparticles via ultrasonic irradiation and their electro-catalytic activity for oxygen reduction reaction, Appl. Catal. A Gen. 560 (2018) 103–110. https://doi.org/10.1016/j.apcata.2018.04.034.

[5] T.A. Revathy, S. Dhanavel, T. Sivaranjani, V. Narayanan, T. Maiyalagan, A. Stephen, Highly active graphene-supported palladium-nickel alloy nanoparticles for catalytic reduction of 4-nitrophenol, Appl. Surf. Sci. 449 (2018) 764–771. https://doi.org/10.1016/j.apsusc.2018.01.280.

[6] J. Liu, C.Q. Sun, W. Zhu, Origin of efficient oxygen reduction reaction on Pd monolayer supported on Pd-M (M=Ni, Fe) intermetallic alloy, Electrochim. Acta. 282 (2018) 680–686. https://doi.org/10.1016/j.electacta.2018.06.041.

[7] W. Che, Y. Ni, Y. Zhang, Y. Ma, Morphology-controllable synthesis of CuO nanostructures and their catalytic activity for the reduction of 4-nitrophenol, J. Phys. Chem. Solids. 77 (2015) 1–7. https://doi.org/10.1016/j.jpcs.2014.09.006.

[8] K. Sahu, R. Singhal, S. Mohapatra, Morphology Controlled CuO Nanostructures for Efficient Catalytic Reduction of 4-Nitrophenol, Catal. Letters. 150 (2020) 471–481. https://doi.org/10.1007/s10562-019-03009-w.

[9] J.S. Riva, G. Pozo-López, A.M. Condó, L.M. Fabietti, S.E. Urreta, Low temperature ferromagnetism in Rh-rich Fe-Rh granular nanowires, J. Alloys Compd. 747 (2018) 1008–1017. https://doi.org/10.1016/j.jallcom.2018.03.091.

[10] J.S. Riva, A. V. Juárez, S.E. Urreta, L.M. Yudi, Catalytic properties of Fe–Pd ferromagnetic nanowires at liquid/liquid interfaces, Electrochim. Acta. 298 (2019) 379–388. https://doi.org/10.1016/j.electacta.2018.12.069.

[11] F. Maillard, S. Schreier, M. Hanzlik, E.R. Savinova, S. Weinkauf, U. Stimming, Influence of particle agglomeration on the catalytic activity of carbon-supported Pt nanoparticles in CO monolayer oxidation, Phys. Chem. Chem. Phys. 7 (2005) 385–393. https://doi.org/10.1039/b411377b.

[12] A. Zare Asadabadi, S.J. Hoseini, M. Bahrami, S.M. Nabavizadeh, Catalytic applications of β-cyclodextrin/palladium nanoparticle thin film obtained from oil/water interface in the reduction of toxic nitrophenol compounds and the degradation of azo dyes, New J. Chem. 43 (2019) 6513–6522. https://doi.org/10.1039/c8nj06449k.

[13] L. Strimbu, J. Liu, A.E. Kaifer, Cyclodextrin-capped palladium nanoparticles as catalysts for the Suzuki reaction, Langmuir. 19 (2003) 483–485. https://doi.org/10.1021/la026550n.

[14] J. Ma, C. Yang, S. Zhu, J. Song, Y. Fu, A Pt and Pd bimetal nanowire based stereoselective sensor for the discrimination of ascorbic acid and isoascorbic acid, Anal. Methods. 10 (2018)

1703–1708. https://doi.org/10.1039/c8ay00300a.

[15] K. Sahu, B. Satpati, S. Mohapatra, Facile Synthesis and Phase-Dependent Catalytic Activity of Cabbage-Type Copper Oxide Nanostructures for Highly Efficient Reduction of 4-Nitrophenol, Catal. Letters. 149 (2019) 2519–2527. https://doi.org/10.1007/s10562-019-02817-4.

[16] K. Sahu, A. Bisht, A. Pandey, A. Dutta, S.A. Khan, R. Singhal, T. Som, S. Mohapatra, RF magnetron sputtered Ag-Cu2O-CuO nanocomposite thin films with highly enhanced photocatalytic and catalytic performance, Appl. Surf. Sci. 517 (2020) 146169. https://doi.org/10.1016/j.apsusc.2020.146169.

[17] O.F. Silva, M.A. Fernández, S.L. Pennies, R.R. Gil, R.H. De Rossi, Synthesis and characterization of an amphiphilic cyclodextrin, a micelle with two recognition sites, Langmuir. 24 (2008) 3718–3726. https://doi.org/10.1021/la702962f.

[18] X.L. Fei, S.L. Tang, R.L. Wang, H.L. Su, Y.W. Du, Fabrication and magnetic properties of Fe-Pd nanowire arrays, Solid State Commun. 141 (2007) 25–28. https://doi.org/10.1016/j.ssc.2006.09.042.

[19] D. Pečko, K.Ž. Rožman, N. Kostevšek, M. Shahid Arshad, B. Markoli, Z. Samardžija, S. Kobe, Electrodeposited hard-magnetic Fe50Pd50 nanowires from an ammonium-citrate-based bath, J. Alloys Compd. 605 (2014) 71–79. https://doi.org/https://doi.org/10.1016/j.jallcom.2014.03.156156.

[20] L.I. Rossi, R.H. de Rossi, Synthesis of FeBr3-cyclodextrin complexes in non-aqueous solution, J. Supramol. Chem. 2 (2002) 509–514. https://doi.org/10.1016/S1472-7862(02)00076-X.

[21] M. V. Slavgorodska, A. Kyrychenko, Adsorption behavior of β-cyclodextrin onto gold nanoparticles, J. Mol. Graph. Model. 94 (2020) 107483. https://doi.org/10.1016/j.jmgm.2019.107483.

[22] L. Zhang, R. He, H.C. Gu, Oleic acid coating on the monodisperse magnetite nanoparticles, Appl. Surf. Sci. (2006). https://doi.org/10.1016/j.apsusc.2006.05.023.

[23] L.B. Devi, A.B. Mandal, Self-assembly of Ag nanoparticles using hydroxypropyl cyclodextrin: Synthesis, characterisation and application for the catalytic reduction of p-nitrophenol, RSC Adv. (2013). https://doi.org/10.1039/c3ra23014g.

[24] J.H. Ennist, E.A. Gobrogge, K.H. Schlick, R.A. Walker, M.J. Cloninger, Cyclodextrin-functionalized chromatographic materials tailored for reversible adsorption, ACS Appl. Mater. Interfaces. 6 (2014) 18087–18097. https://doi.org/10.1021/am504975y.

[25] A.Z.M. Badruddoza, Z.B.Z. Shawon, W.J.D. Tay, K. Hidajat, M.S. Uddin, Fe 3O 4/cyclodextrin polymer nanocomposites for selective heavy metals removal from industrial wastewater, Carbohydr. Polym. 91 (2013) 322–332. https://doi.org/10.1016/j.carbpol.2012.08.030.

[26] M. Zhang, L. Zhu, C. He, X. Xu, Z. Duan, S. Liu, M. Song, S. Song, J. Shi, Y. Li, G. Cao, Adsorption performance and mechanisms of Pb(II), Cd(II), and Mn(II) removal by a β-cyclodextrin derivative, Environ. Sci. Pollut. Res. 26 (2019) 5094–5110. https://doi.org/10.1007/s11356-018-3989-4.

[27] R. Mrówczyński, A. Jędrzak, K. Szutkowski, B. Grześkowiak, E. Coy, R. Markiewicz, T. Jesionowski, S. Jurga, Cyclodextrin-Based Magnetic Nanoparticles for Cancer Therapy, Nanomaterials. 8 (2018) 170. https://doi.org/10.3390/nano8030170.

[28] B. Wang, X. Yang, L. Ma, L. Zhai, J. Xuan, C. Liu, Z. Bai, Ultra-high efficient pH induced selective removal of cationic and anionic dyes from complex coexisted solution by novel

amphoteric biocomposite microspheres, Sep. Purif. Technol. 231 (2020) 115922. https://doi.org/10.1016/j.seppur.2019.115922.

[29] S. Bahadorikhalili, L. Ma'mani, H. Mahdavi, A. Shafiee, Copper supported B-cyclodextrin functionalized PEGylated mesoporous silica nanoparticle -graphene oxide hybrid: An efficient and recyclable nano-catalyst for straightforward synthesis of 2-arylbenzimidazoles and 1,2,3-triazoles, Microporous Mesoporous Mater. 262 (2018) 207–216. https://doi.org/10.1016/j.micromeso.2017.11.046.

[30] G. Greczynski, L. Hultman, X-ray photoelectron spectroscopy: Towards reliable binding energy referencing, Prog. Mater. Sci. 107 (2019) 100591. https://doi.org/10.1016/j.pmatsci.2019.100591.

[31] L. Chen, A. Yelon, E. Sacher, X-ray photoelectron spectroscopic studies of Pd nanoparticles deposited onto highly oriented pyrolytic graphite: Interfacial interaction, spectral asymmetry, and size determination, J. Phys. Chem. C. 115 (2011) 7896–7905. https://doi.org/10.1021/jp1119266.

[32] K.K. Dilorenzo, R.M. Gilbert, P.E. Hoggard, Near-UV photolysis of μ-dibromotetrabromodipalladate(II) in chloroform, J. Coord. Chem. 63 (2010) 558–567. https://doi.org/10.1080/00958970903582696.

[33] W.R. Mason, H.B. Gray, Electronic Structures of Square-Planar Complexes, J. Am. Chem. Soc. 90 (1968) 5721–5729. https://doi.org/10.1021/ja01023a012.

[34] P. Zhao, X. Feng, D. Huang, G. Yang, D. Astruc, Basic concepts and recent advances in nitrophenol reduction by gold- and other transition metal nanoparticles, Coord. Chem. Rev. 287 (2015) 114–136. https://doi.org/10.1016/j.ccr.2015.01.002.

[35] Y. Mei, G. Sharma, Y. Lu, M. Ballauff, M. Drechsler, T. Irrgang, R. Kempe, High catalytic activity of platinum nanoparticles immobilized on spherical polyelectrolyte brushes, Langmuir. 21 (2005) 12229–12234. https://doi.org/10.1021/la052120w.

[36] M.V. Bravo, O.F. Silva, C. Adam, A.M. Granados, A simple way to prepare palladium nanoparticles decorated with cyclodextrins and ionic liquid. The effects of coating on the catalytic activity and colloidal stability, J. Mol. Liq. 304 (2020) 112725.

[37] T. Yao, T. Cui, X. Fang, F. Cui, J. Wu, Preparation of yolk-shell FexOy/Pd@mesoporous SiO2 composites with high stability and their application in catalytic reduction of 4-nitrophenol, Nanoscale. 5 (2013) 5896–5904. https://doi.org/10.1039/c3nr01470c.

[38] S. Gu, S. Wunder, Y. Lu, M. Ballauff, R. Fenger, K. Rademann, B. Jaquet, A. Zaccone, Kinetic analysis of the catalytic reduction of 4-nitrophenol by metallic nanoparticles, J. Phys. Chem. C. (2014). https://doi.org/10.1021/jp5060606.

[39] Z. Meng, G. Li, N. Zhu, C.L. Ho, C.W. Leung, W.Y. Wong, One-pot synthesis of ferromagnetic FePd nanoparticles from single-source organometallic precursors and size effect of metal fraction in polymer chain, J. Organomet. Chem. 849–850 (2017) 10–16. https://doi.org/10.1016/j.jorganchem.2017.06.006.

[40] S. Fountoulaki, V. Daikopoulou, P.L. Gkizis, I. Tamiolakis, G.S. Armatas, I.N. Lykakis, Mechanistic studies of the reduction of nitroarenes by NaBH4 or hydrosilanes catalyzed by supported gold nanoparticles, ACS Catal. (2014). https://doi.org/10.1021/cs500379u.